JOURNAL OF MATERIALS SCIENCE 27 (1992) 6755–6764

Structure and thermal evolution of Ag–Ni multilayers

WANG YUANSHENG*, J. P. SIMON
LTPCM, ENSEEG, Institut National Polytechnique de Grenoble, BP 75, 38402 St-Martin-d'Héres, France

The structure of Ag–Ni multilayered samples with different layer thicknesses and their evolution during annealing have been investigated by transmission electron microscopy and X-ray diffraction. For all samples, there is a dominant [111] texture in the growth direction. Nevertheless, this texture axis deviates from pure [111] with a scatter of about 20°. Increasing the layer thickness enhances the proportion of pure [111] texture. At the beginning of the deposition, the grains show random in-plane orientations; with further deposition of bilayers, an in-plane texture is formed. The annealing induces strain relaxation, grain growth and coarsening; the latter finally destroys the layered structure. The multilayer stability increases with the layer thickness.

1. Introduction

There has been great interest in metallic multilayers in recent years, stimulated mainly by the novel structures and properties of these materials [1–3]. The very thin individual layers may exhibit different characteristics from those of bulk materials; moreover, the interaction between two elemental layers will probably induce new effects. Some authors have studied the influence of the layer thickness on the structure [4], and on the elastic [5] and magnetic [6] properties of multilayered materials.

The individual layer structure, and the structural correlations between two elemental layers, play important roles in the thermal stability and physical properties of multilayered systems. The present paper deals with a study of the structure and the thermal evolution of Ag–Ni multilayers prepared by cathodic sputtering. To our knowledge, up to now there have been few detailed studies on this system. Our interest was motivated by the facts that, in the bulk state, the Ag–Ni system has a very limited mutual solubility [7] and both metals have the f.c.c. lattice structure, but with a large difference in lattice parameters ($a_{Ag} = 0.4085$ nm and $a_{Ni} = 0.3523$ nm, $f = \Delta a/a = 0.15$) [8]. It is thus possible to study a periodic structure with sharp concentration modulations and a large lattice mismatch at interfaces. The annealing of this system will affect the interfacial coherency, the grain size and the texture. All these aspects will be emphasized in the following.

2. Experimental procedure

2.1. Samples

Ag–Ni multilayers were prepared at CENG (Centre d'Etudes Nucléaires de Grenoble) with d.c. sputtering, alternately depositing Ag and Ni layers on float glass [9]. Assuming [1 1 1] texture with the texture axis perpendicular to the layers, the samples are denoted as N_{Ag}/N_{Ni}, i.e. 5/5, 8/8, 20/20 and 40/40 respectively according to the nominal number (N_{Ag} and N_{Ni}) of atomic planes in Ag and Ni layers. The substrate temperature was 100 K for 5/5, 8/8 and 40/40, and 300 K for 20/20. The total thickness of the film was usually about 5 μm. At such large thicknesses, the samples could be detached from their substrate. In such substrate-free samples thin foils for transmission electron microscopy (TEM) plane-view observations could be prepared directly by electro-polishing and ion-milling techniques. Besides these 5 μm thick samples, some samples with film thicknesses of about 35 nm (deposited on mica) were also studied.

2.2. Experimental methods

2.2.1. *TEM* in situ *observation*

TEM experiements were carried out with a Jeol-200CX transmission electron microscope. The observations were performed mainly with plane-view samples; thus the electron diffraction patterns contain in-plane structural information. In addition, TEM observation of a cross-sectional sample (40/40, total thickness ~ 510 nm) with incident electron beam parallel to the layers was also performed.

The *in situ* heating in the microscope stage was a cumulative isothermal annealing of 30 min with a temperature step of 50 °C, beginning from room temperature.

For TEM plane-view observations, thin foils from 5 μm multilayers were prepared first by double-jet electro-polishing with 15% nitric acid + methanol at − 40 °C, and then by ion-milling to get large transparent areas. The 35 nm thick multilayer films were separated from the mica in water, taking advantage of

*On leave from Chemistry Department, Fuzhou University, People's Republic of China.

0022–2461

the strong water capillarity, and then collected on Cu grids and observed directly. Samples for TEM cross-sectional observation were prepared by the method described by Yang *et al.* [10].

In order to measure the evolution of lattice spacing during the *in situ* heating, a precise calibration of the diffraction pattern was necessary. Thus pure Cu was deposited on the thin foil by a standard evaporation.

2.2.2. X-ray diffraction

The X-ray diffraction experiments were carried out on a Siemens D500 diffractometer using $CuK_{\alpha 1}$ radiation ($\lambda = 0.15406$ nm) in reflection geometry (with the scattering vector perpendicular to the planes of the layer). Thus the X-ray diffraction pattern provided information about the artificial periodicity and other interplanar structural features.

For X-ray diffraction measurements, different multilayered samples were treated by cumulative annealing in a vacuum to the times and temperatures indicated in Fig. 8 below. Samples were 3 mm diameter discs which had been treated in the heating stage of the TEM in order to be fully comparable with the *in situ* TEM observations.

3. Results and discussion

3.1. TEM observations

3.1.1. As-deposited states: texture

Fig. 1a–d shows the electron diffraction patterns of 5/5, 8/8, 20/20 and 40/40 samples, respectively. First let us examine the pattern of the 20/20 sample. According mainly to the d spacings, the diffraction rings are indexed as (from low d spacing to high d spacing): Ni(2 2 0), Ag(2 2 0), Ni(1 1 1), Ag(1 1 1) and Ag(2 2 4)/3. There is no (2 0 0) diffraction. For all of the samples, the diffraction rings are not uniform in intensity but divided into arcs, with Ag and Ni diffraction arcs always in the same directions.

The Ag(2 2 4)/3 forbidden diffraction is formed when the number of (1 1 1) close-packed Ag atomic planes parallel to the interfaces is $N = 3n \pm 1$ (n is an integer number); i.e., besides the complete f.c.c. unit cells (when $N = 3n$, the layer consists of an integer number of f.c.c. unit cells) there are "surplus" atomic planes in each Ag layer. These surplus atomic planes induce the structural factor of the (2 2 4)/3 reflection of the Ag layer to be non-zero. Thus the forbidden ring is a signature of the [1 1 1] texture of the multilayers. Such (2 2 4)/3 forbidden reflections have already been observed in very thin (1 1 1) films [11] and in Ag–Ni multilayers [12]. The formation of such forbidden diffraction has been discussed by Cherns [13]. The [1 1 1] textured growth of Ag–Ni multilayers was already quoted by Rodmacq [9], and it is a fairly common situation for the layered growth of two f.c.c. metallic elements.

Comparing the four diffraction patterns in Fig. 1, the intensities of Ag(2 2 4)/3 and Ni(2 2 4)/3 forbidden rings increase with the layer thickness. It seems to indicate that, with an increase of the layer thickness, the [1 1 1] texture gets relatively stronger; in other

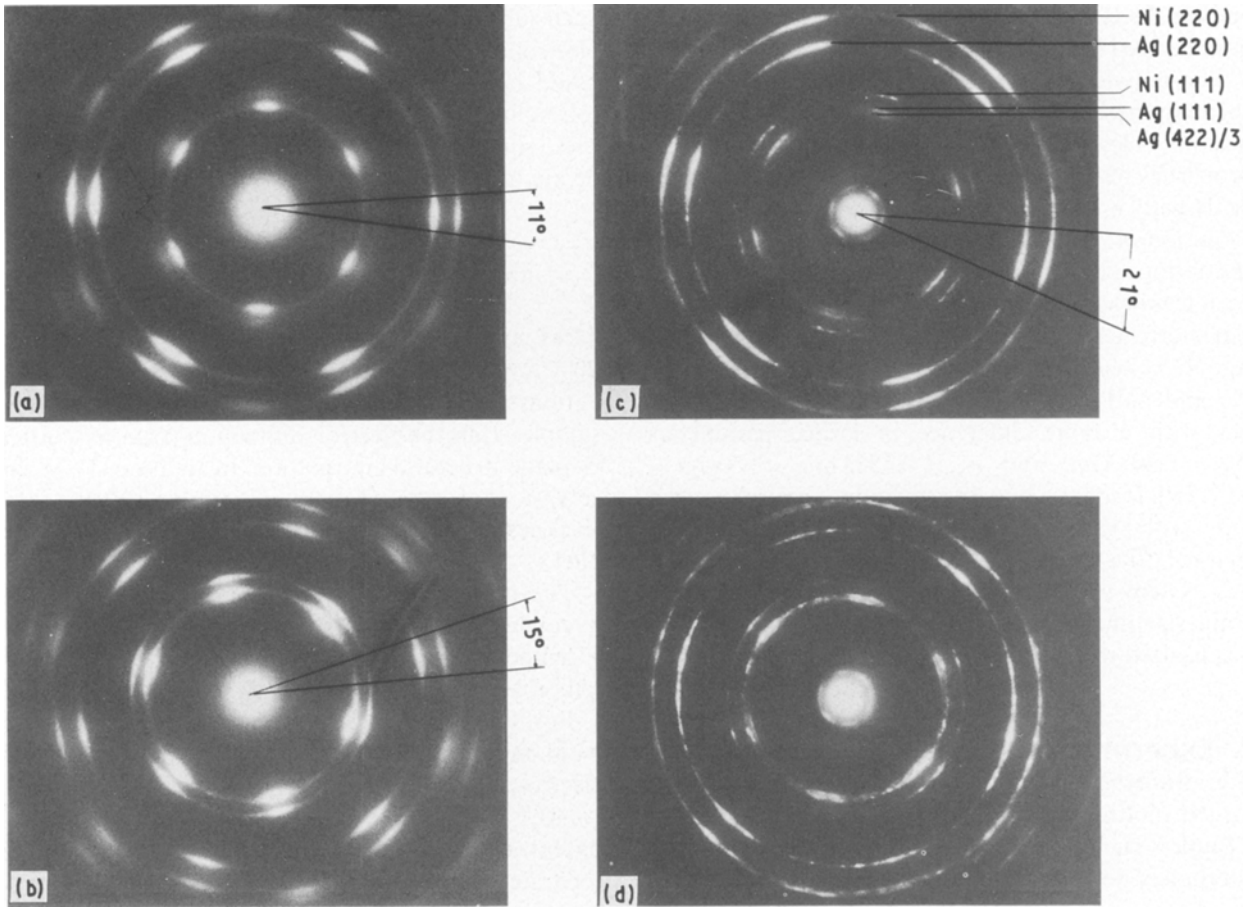

Figure 1 Electron diffraction patterns of as-deposited samples with film thickness ~ 5 μm: (a) 5/5, (b) 8/8, (c) 20/20, (d) 40/40.

words, the proportion of pure [1 1 1] texture is enhanced or the spread angle of the [1 1 1] texture axis is more restricted.

If the sample was completely [1 1 1] textured there would be no (1 1 1) diffraction, but the pattern shows rather strong Ag(1 1 1) and Ni(1 1 1) rings. Moreover, these (1 1 1) rings exhibit six arcs with sixfold symmetry. It is well known that in a single set of f.c.c. lattice the (1 1 1) diffraction never exhibits six-fold symmetry. This puzzling result was analysed following two directions.

First, let us examine the stereographic projection of the cubic lattice. Near the [1 1 1] axis there are [1 2 1], [1 1 2] and [2 1 1] axes exhibiting threefold symmetry with each other around the [1 1 1] axis. The angles between [1 1 1] and these three ⟨1 1 2⟩ axes are the same, i.e. $\theta = 19.47°$, which is the smallest among the angles between [1 1 1] and other directions. It seems that in these samples, besides the [1 1 1] texture, there is some extent of ⟨1 1 2⟩ texture appearing as a result of the anisotropic angle spread of the [1 1 1] texture axis. Such a spread has been observed by high-resolution electron microscopy on an Ag–Ni cross-sectional sample [14]. Its origin may be due to the steps necessary to achieve the relaxation of the Ag–Ni interfaces by misfit dislocations. Three sets of ⟨1 1 2⟩ textured grains with texture axes exhibiting threefold symmetry around the [1 1 1] axis form the threefold (1 1 1) arcs. The [1 1 1] and the ⟨1 1 2⟩ textured grains share the same (2 2 0) arcs, so that they have the same ⟨2 2 0⟩ in-plane orientations.

Since for the f.c.c. lattice the (1 1 1) plane is the most close-packed plane, [1 1 1] texture is thus the most energy-favourable. The large angular spread of the texture axis would enhance the total energy of the system. With further progress of deposition of a layer, it is reasonable that the angular spread tends to shrink with the layer thickness.

Secondly, considering the very short periodicity of these multilayers, the appearance of (1 1 1) diffraction rings may also be explained by the higher-order Laue zone diffraction phenomena of [1 1 1] textured multilayers. Since the elemental layers in the samples are very thin, the reciprocal lattice spots appear as elongated rods with the elongation direction perpendicular to the layers. Thus it is possible that the Ewald sphere cuts the $1\,1\,\bar{1}^*$ reciprocal rods at the first-order Laue zone which gives $(1\,1\,\bar{1})$ diffraction. The angle between $[1\,1\,\bar{1}]^*$ directions and the $(1\,1\,1)^*$ plane is 19.47°. The TEM specimen-tilting experiment shows that, when the specimen is tilted around an axis from 0 to about 20° (the angle between the incident electron beam and the normal to the multilayers), the (1 1 1) diffraction in the direction perpendicular to this axis gets continuously stronger with increasing tilting angle. Then it tends to be weaker with further tilting. This result supports the above interpretation of (1 1 1) diffractions. The length of the $1\,1\,\bar{1}^*$ reciprocal rods gets shorter as the layer thickness is increased. It may also explain why the intensity of (1 1 1) diffraction arcs decreases as the layer thickness is increased (see Fig. 4 below).

Fig. 2 shows the TEM bright-field image and the corresponding electron diffraction pattern of cross-sectional sample (40/40, total thickness ~ 510 nm). The bright-field image shows clearly the periodic layered structure. The measured bilayer length is about 21 nm. In the diffraction pattern, along the perpendicular direction of the layers the (1 1 1) spots appear much stronger than the ones corresponding to the other directions, confirming the [1 1 1] textured growth along the perpendicular direction.

Summarizing the discussion above, the growth of Ag–Ni multilayers is [1 1 1] textured; the texture axis may spread anisotropically to form ⟨1 1 2⟩ texture to some extent; with increase of the layer thickness, this angular spread of the texture axis becomes smaller.

In the 40/40 pattern there is a strong ring near the non-diffracted beam with a d spacing of about 1 nm. This d spacing agrees with the calculated spacing of the moiré fringes formed by the parallel Ag(2 2 0) and Ni(2 2 0) lattice planes ($d = 0.92$ nm), showing that it is

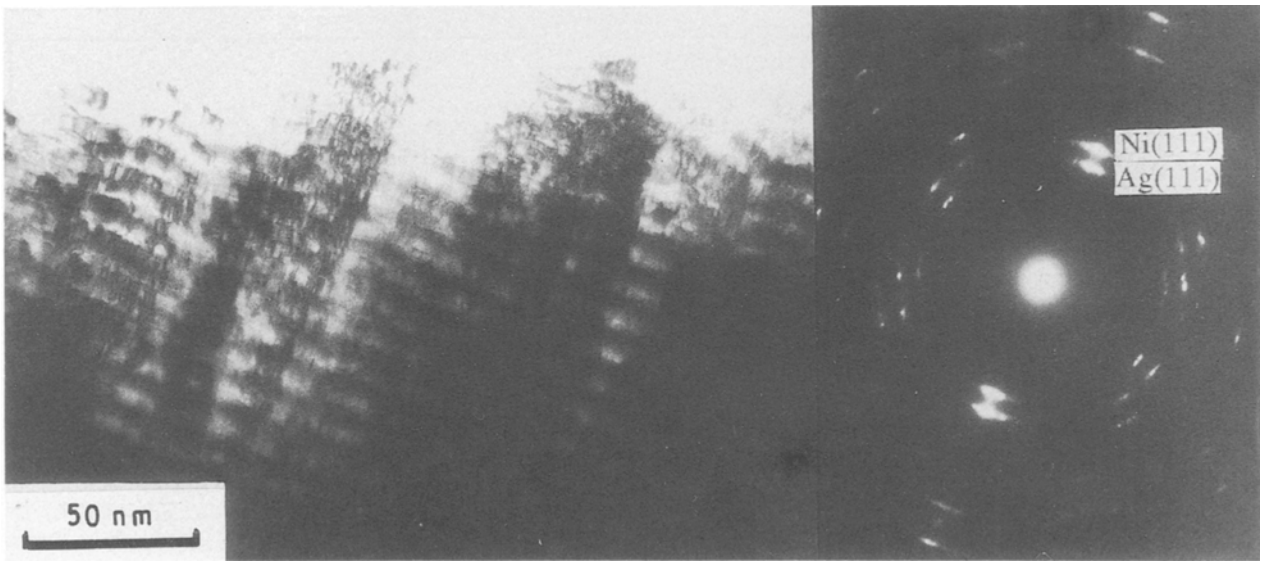

Figure 2 TEM bright-field image and corresponding electron diffraction pattern of cross-sectional sample (40/40 Ag–Ni multilayers with film thickness ~ 510 nm).

the contribution of double diffraction from Ag(2 2 0) and Ni(2 2 0) planes. Such double diffraction has also been observed in Au–Ni superlattice films [15]. It indicates that a large proportion of Ag and Ni grains in the same column have the same orientations. This ring is absent in 5/5 samples but is detected in 8/8 samples, although the intensity is very low (Fig. 1); when the layer thickness increases, this double diffraction ring gets stronger. As interpretation, when the lattice planes of two elements are all undistorted and perpendicular to the interface, the double diffraction results from a quasi-dynamic interaction of the electron wave with the synthetic perfect crystal. The absence of double diffraction in the 5/5 pattern is probably due to the large coherency strains induced by the large lattice mismatch between two layers. The formation of double diffraction on increasing the layer thickness is the result of the decrease of lattice strain due to the generation of misfit dislocations at the interfaces. The lattice parameters (see section 3.1.2 below) and the X-ray diffraction peak widths (section 3.2) are consistent with this interpretation. Thus we get the conclusion that the interfacial coherency, and hence the lattice strain of the sample, decreases as the layer thickness increases.

Besides this texture perpendicular to the layers, the anisotropy of intensities of diffraction rings indicates that there is an in-plane texture too; Ag and Ni grains in different layers keep the same in-plane orientations, as was already pointed out [9]. The diffraction arcs show an orientational spread for the in-plane texture. The spread angle of (2 2 0) diffraction arcs is about 11, 15 and 21° for 5/5, 8/8 and 40/40 samples, respectively; this angle increases with the layer thickness. It seems that during the layer growth, there is some correlation between the orientations of the new grain nuclei, but, this correlation being weak, there is a global increase of the angle scatter. (Let us recall that the diffraction pattern, taken in a selected area of about 1 μm^2, is the contribution of more than 10^4 grains in each layer.) For all samples, when we laterally displace the selected area, the orientation of arcs in the electron diffraction pattern changes continuously. This can be explained by the following morphological description: the multilayers consist of columns perpendicular to the layer; in each column the in-plane orientation is the same; neighbouring columns show somewhat different but correlated in-plane orientations. A columnar structure has already been found by Dohnomae *et al.* in Au–Ni multilayers [15].

To study the influence of the total bilayer number on the structure, 5/5 and 20/20 samples with a total thickness of about 35 nm have been investigated by TEM. Fig. 3 shows the electron diffraction pattern of such a 20/20 sample. Comparing Fig. 3 with Fig. 1c, in the former case (35 nm) all the diffraction rings are homogeneous in intensity, while in the latter case (5 μm) all the rings are divided into arcs. We have also prepared thin TEM foils from the "lower" side (the side in contact with the substrate) and the "up" side (the side exposed to the air) of 5 μm thick 20/20 samples by single-jet electro-polishing. The electron diffraction pattern from the "lower" side of the foil is

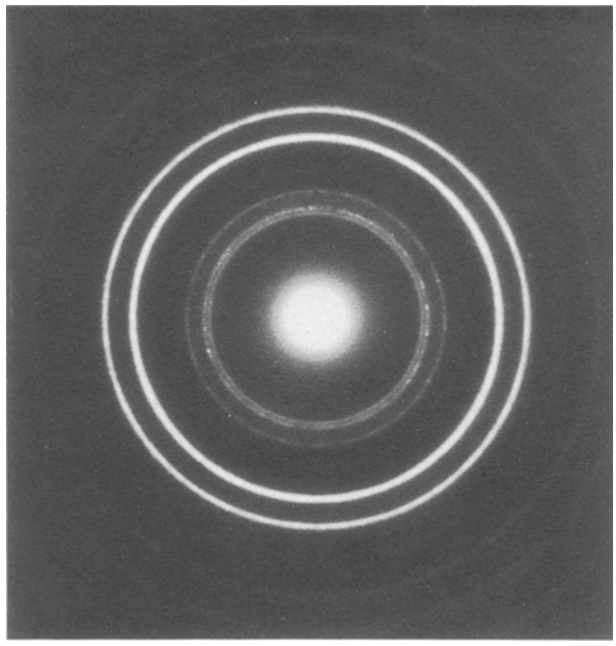

Figure 3 Electron diffraction pattern of as-deposited 20/20 Ag–Ni multilayers with film thickness ~ 35 nm.

similar to that of the 35 nm thick film, and that from the "up" side foil is similar to that from the centre of the 5 μm sample (equivalent to Fig. 1c). Thus, on increasing the bilayer number the in-plane orientations tend from random to anisotropic textured. It is thus proposed that, in the first deposited layers, the crystal nucleation is at random in about the (1 1 1) plane (only [1 1 1] texture in the growth direction); then, as deposition of layers proceeds, it establishes progressively an in-plane texture, probably due to a correlation between neighbouring grains which tend to have the same orientation: then, at each new nucleation, the grain chooses an orientation close to the mean orientation of its neighbours.

3.1.2. As-deposited state: elastic strains

The parallel lattice spacings of Ag and Ni phases for the as-deposited state are given in Fig. 4: compared to

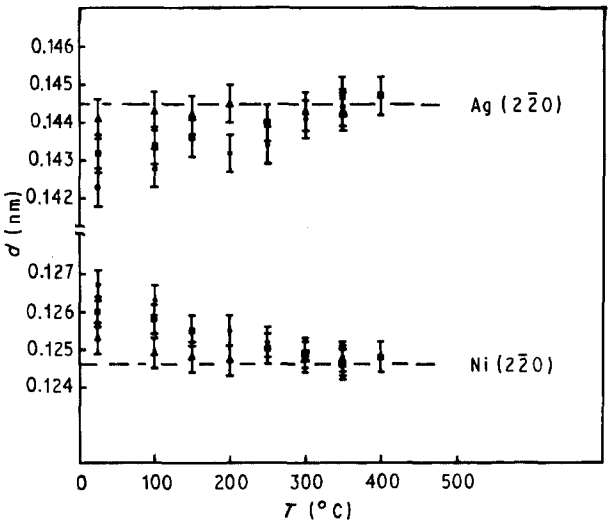

Figure 4 Evolution of Ag(2 2 0) and Ni(2 2 0) lattice spacings of Ag–Ni multilayers with different numbers of atomic plane in each layer: (●) 5/5, (■) 8/8 and (▲) 40/40, during *in situ* heating in TEM.

the bulk values, the Ag(2 2 0) lattice spacing is compressed while the Ni(2 2 0) lattice spacing is expanded. The lattice strain increases with decreasing layer thickness. In 5/5 samples, although the lattice is heavily strained to accommodate the large mismatch between Ag and Ni lattices, the interfaces between two layers have not yet reached coherency but are only semi-coherent, since Ag(2 2 0) and Ni(2 2 0) planes still have different spacings. From elastic calculations, in the coherent state the (2 2 0) lattice plane spacing should be $d = 0.1303$ nm (since Ag and Ni layers have different shear moduli and thicknesses, this d value does not equal the mean value of Ag(2 2 0) and Ni(2 2 0) lattice spacings in bulk states). This d value is between the two values (0.1423 and 0.1267 nm) for Ag(2 2 0) and Ni(2 2 0) lattice spacings, respectively, of 5/5 samples in the as-deposited state.

There should be misfit dislocations at the interfaces to accommodate the residual mismatch. For multilayer systems, there exists theoretically a critical thickness for the generation of misfit dislocations at the interfaces [16, 17]: below this thickness the interfaces are coherent and the material is strained, while above it misfit dislocations are created and the material is partially or fully relaxed, giving semi-coherent or incoherent interfaces. Elastic calculations following Matthews and Blakeslee [16] gives a critical thickness in Ag–Ni multilayers of about 0.8 nm. This thickness is less than the layer thickness of 5/5 samples.

3.1.3. *In situ* heating: lattice relaxation

In order to reveal the lattice relaxation process of multilayers with different layer thicknesses, the evolution of the parallel lattice spacings of Ag and Ni phases has been measured during TEM *in situ* heating. The diffraction results, with Cu as calibration, are shown in Fig. 4.

From Fig. 4, the strained lattices in 5/5, 8/8 and 40/40 samples relax progressively toward the equilibrium bulk states with increasing annealing temperature. The relaxations begin at rather low temperatures: at 100 °C, to a noticeable amount for the three samples. When the temperature rises to about 350 °C the strains are fully relaxed.

3.1.4. *In situ* heating: grain growth and coarsening

Fig. 5 shows bright-field images and the corresponding electron diffraction patterns of a 5/5 sample for three states during the *in situ* annealing: i.e. before heating and heated *in situ* to 300 and 450 °C. The evolution sequence will be presented in more detail in the following: before heating (Fig. 5a), the bright-field image shows a lot of fine wavy contrasts; the grain contours are unidentifiable. Attempts by dark-field imaging to distinguish the grains also failed. This is probably caused by the fact that the grains are strongly textured in both the perpendicular and in-plane directions. Neighbouring grains have similar orientations, thus the difference of diffraction contrast between them is very small in bright-field images. Moreover, the diffraction arcs used for the formation of dark-field images give contributions from all of the textured grains, so we cannot individualize them.

There is no noticeable evolution in either bright-field images or diffraction patterns until about 200 °C. At 200 °C, the double diffraction ring from Ag(2 2 0) and Ni(2 2 0) planes appears while some moiré fringes can be seen in bright-field images as the result of lattice strain relaxations. The intensity of this double diffraction ring gets stronger with further increase of the temperature, showing the progress of the relaxation. When the temperature reaches 250 °C some small grains with clear contours appear and grow among the matrix. Meanwhile, Ag(1 1 1) and Ni(1 1 1) diffraction rings tend to be weaker. They indicate the beginning of grain growth. At 300 °C (Fig. 5b) many small grains are densely distributed in the sample with regular moiré fringes on most of them. In the diffraction pattern, Ag(1 1 1) and Ni(1 1 1) diffraction rings become weaker and, simultaneously, the double diffraction ring becomes very strong, indicating that relaxation and growth processes are partially overlapped. When the temperature reaches the 350–400 °C range, there is a drastic coarsening process of grains over the whole sample. At a temperature of 450 °C (Fig. 5c) the contrast on most of the grains is very flat and the grain sizes are so large that the grains extend over the whole foil thickness. This has been proved by a compositional analysis of individual grains with scanning transmission electron microscopy. Now the periodic layered structure of the film has been completely destroyed.

Fig. 6 shows the structural evolution of a 40/40 sample. Before heating (Fig. 6a) the bright-field image shows complex wavy contrasts; a lot of moiré fringes with a fringe spacing of about 1 nm can be seen everywhere. The grain contours are still unidentifiable. These features do not change during heating up to 300 °C. When the temperature reaches 300 °C (Fig. 6b) some grains appear and grow slowly among the wavy matrix. The double diffraction ring is as strong as before: there is no significant change in the interfacial coherency. The sixfold Ag(1 1 1) and Ni(1 1 1) spots are still rather strong. When the temperature reaches about 450 °C, a drastic grain coarsening occurs. The temperatures for the beginning of grain growth and coarsening are higher in 40/40 samples than in 5/5 samples. This shows that the stability of the system has been improved. At 500 °C (Fig. 6c) the grains occupy the whole film with grain thicknesses equal to the foil thickness; the layered periodicity has disappeared.

In situ heating observations reveal that the structural evolution behaviour of 8/8 samples is similar to that of 5/5 samples, while that of 20/20 samples is relatively near that of 40/40 samples.

Similar relaxation, grain growth and coarsening behaviour occur during *in situ* heating experiments of 35 nm samples. Nevertheless, in 35 nm samples, whether in as-deposited or annealed states, the in-plane grain sizes can be identified from dark-field images. This is due to the fact that there is no in-plane texture in these samples. The in-plane orientations of

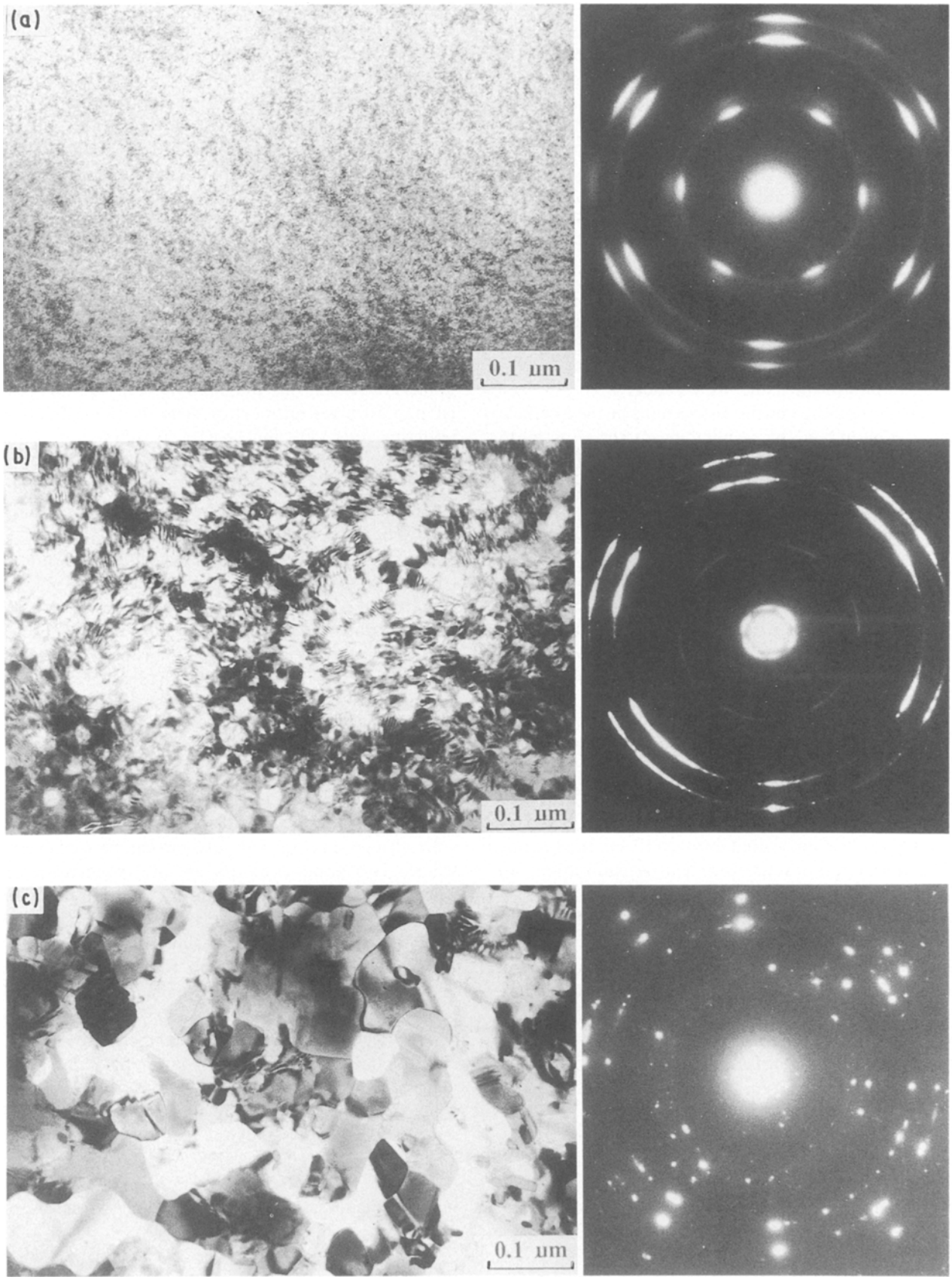

Figure 5 TEM bright-field images and electron diffraction patterns of 5/5 samples showing the effects of *in situ* annealing: (a) as-deposited state; (b) 300 °C, 30 min; (c) 450 °C, 30 min.

grains being at random, grains with different in-plane orientations give diffraction in different directions, and thus can be identified by dark-field images. Therefore it is possible to make *in situ* observations of grain growth during the annealing. From dark-field images shown in Fig. 7 we see that for a 35 nm 8/8 sample in the as-deposited state, the lateral grain sizes are in the range of ≤ 20 nm. After isothermal annealing at 250 °C for 420 min the grains grow to ≤ 45 nm. The layered periodicity is still maintained, as indicated by

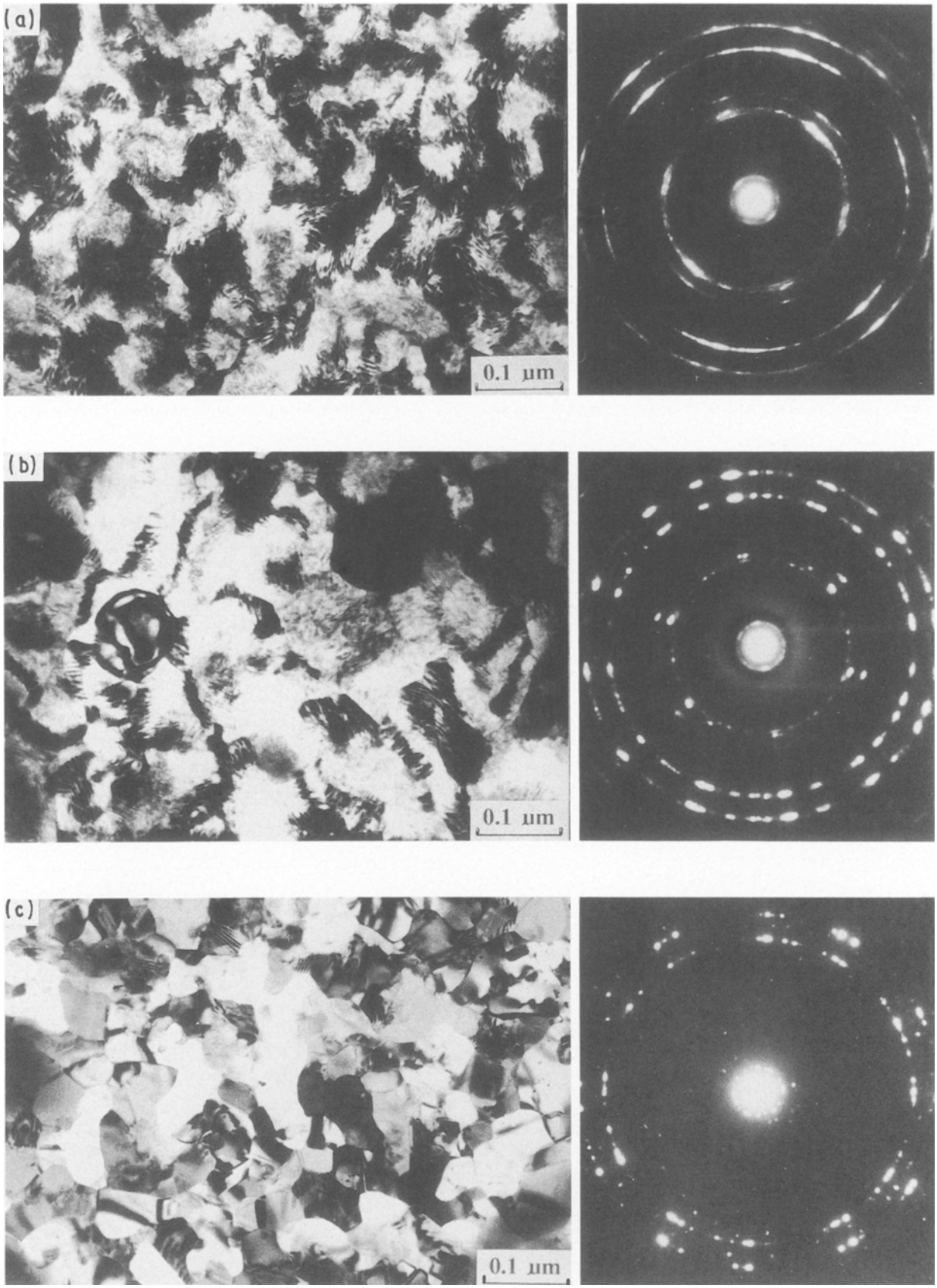

Figure 6 TEM bright-field images and electron diffraction patterns of 40/40 samples showing the effects of *in situ* annealing: (a) as-deposited state; (b) 300 °C, 30 min; (c) 500 °C, 30 min.

persisting forbidden rings in the electron diffraction pattern.

It seems that the destratification is mainly due to a drastic coarsening of grains; the grain growth which appears before the drastic coarsening has no significant influence on the layered structure.

3.2. X-ray diffraction

X-ray diffraction curves for 5/5, 8/8 and 40/40 samples are shown in Fig. 8. For all of these samples, in the as-deposited state there are several satellite peaks near the Ag(1 1 1) and Ni(1 1 1) peak positions, as already studied in detail by Rodmacq [9]. These satellite

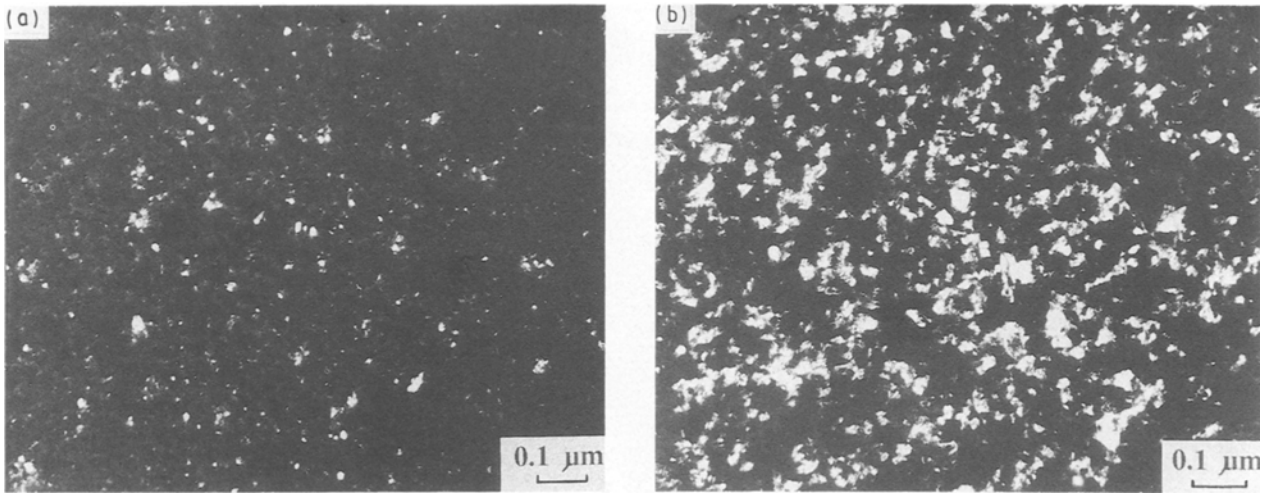

Figure 7 TEM dark-field images of 35 nm 8/8 samples showing grain sizes: (a) as-deposited; (b) isothermally annealed at 250 °C for 420 min.

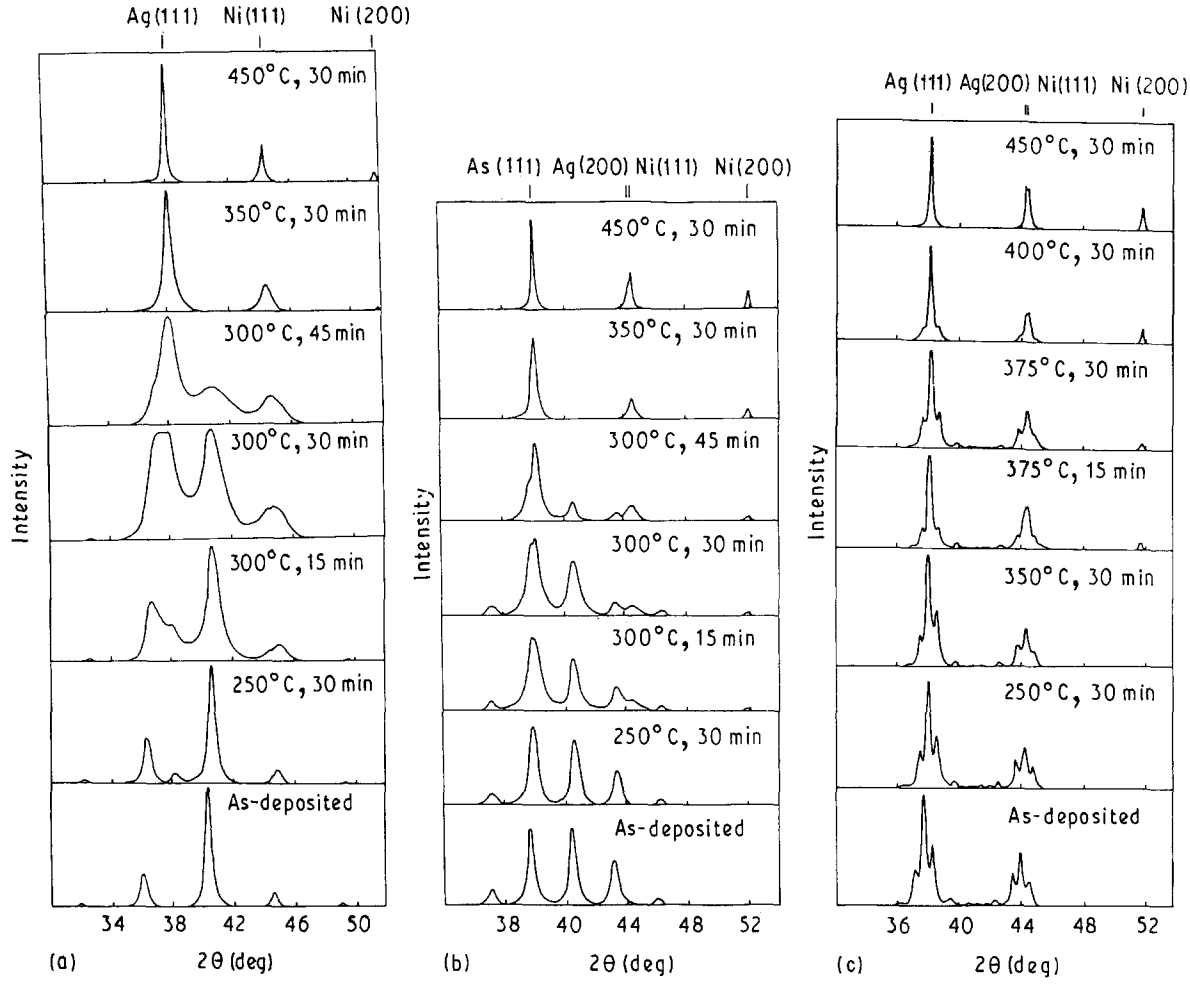

Figure 8 X-ray diffraction spectra of Ag–Ni samples annealed in different states: (a) 5/5 sample, (b) 8/8 sample, (c) 40/40 sample.

peaks are the results of the modulation of artificial periodicity along the perpendicular direction. In contrast, diffraction is absent in the (2 0 0) or (2 2 0) Bragg angle ranges. This confirms the dominant [1 1 1] texture of the samples.

From measurements of the X-ray satellite peak width after correction for the instrumental width, the average perpendicular coherent length of 5/5, 8/8 and 40/40 as-deposited samples is determined to be 32, 29 and 59 nm, respectively, i.e. about 14, 8 and 3 times the bilayer thickness. In other words, the average perpendicular coherent length covers 27, 15 and 5 interfaces for 5/5, 8/8 and 40/40 samples, respectively. It seems that if the interfacial coherency is improved, more interfaces can be included in the coherent length.

Different X-ray diffraction patterns during the thermal evolution are shown in Fig. 8. There are large changes of widths and intensities of the satellite peaks. Their widths tend to be broader (Fig. 9) while their intensities tend to be diminished during annealing.

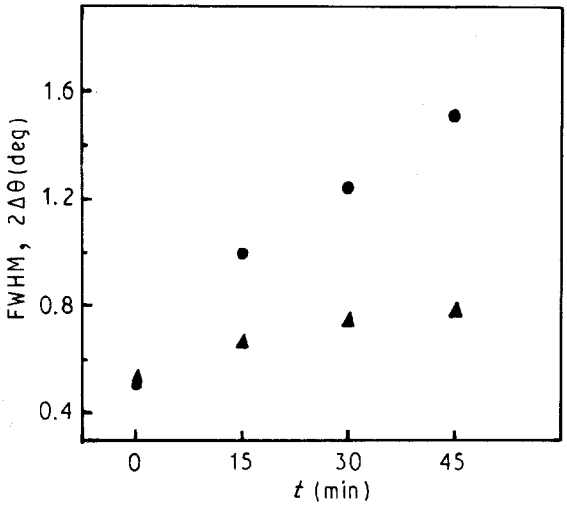

Figure 9 Evolution of X-ray satellite diffraction peak widths (FWHM) of (●) 5/5 and (▲) 8/8 samples during isothermal annealing at 300 °C.

This is likely to follow the "layer coarsening process" during which the thicknesses of the individual layers changes by atomic diffusion: some of the layers get thinner and finally disappear while others become thicker, so reducing the total interfacial energy of the system. This diffusion of atoms from one layer to another across the other elemental layer has been modelled as a "uniform coarsening process" as described by Langer [18] or a "receding fault line coarsening process" as described by Graham and Kraft [19]. Both processes induce a spread of the bilayer thicknesses. At low temperatures, the atomic diffusion is most likely along grain boundaries. Ag and Ni non-miscibility does not favour bulk diffusion. Peak broadening of the 5/5 sample at 250 °C proceeds faster than that of the 8/8 sample, while no visible evolution in the 40/40 sample is detected. The diffusion length for the "coarsening" process is probably proportional to or at least correlated with the layer thickness. When this kind of coarsening (or destratification) has proceeded to such an extent that Ag and Ni grains have sufficient sizes to destroy the layered periodicity, these satellite peaks disappear and the remaining peaks are Ag(1 1 1) and Ni(1 1 1) peaks. The temperature range of the destratification is 250–350 °C for 5/5 and 8/8 samples and 350–450 °C for the 40/40 sample. The stability of the periodic layered structure increases with the layer thickness.

Besides the width and intensity, the position of the satellite peaks also changes during annealing: they shift slightly to higher angles. The average interplanar spacings of 5/5 and 8/8 samples are plotted in Fig. 10 as a function of annealing time for isothermal annealing at 300 °C. The average interplanar spacing decreases with the annealing time, and by an amount more important in 5/5 samples than in 8/8 samples. The contraction of the interplanar spacing can reasonably be attributed to lattice strain relaxation of the samples. From Fig. 10, it appears that after 45 min annealing at 300 °C the average interplanar spacing does not reach the theoretical value d_t given by

$$d_t = \frac{N_{Ag}d_{Ag} + N_{Ni}d_{Ni}}{N_{Ag} + N_{Ni}} = \frac{d_{Ag} + d_{Ni}}{2} = 0.2196\,\text{nm}$$

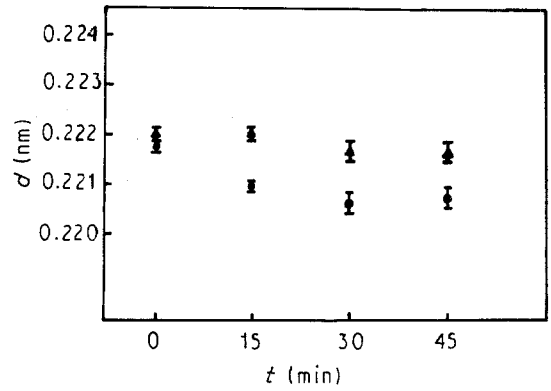

Figure 10 Evolution of average interplanar spacings of (●) 5/5 and (▲) 8/8 samples during isothermal annealing at 300 °C, determined from X-ray diffraction measurements.

(taking $N_{Ag} = N_{Ni}$). One reason could be that the lattices have not been fully relaxed, but it is more probably due to the fact that we do not have exactly $N_{Ag} = N_{Ni}$ for both 5/5 and 8/8 samples. From the previous X-ray diffraction study by Rodmacq [9], the values of $N_{Ag} = 5.46$ and $N_{Ni} = 4.58$ give the best simulation of the satellite pattern for the 5/5 sample, while for the 8/8 sample $N_{Ag} = 8.34$ and $N_{Ni} = 7.20$. Thus the average interplanar spacings of 5/5 and 8/8 samples when fully relaxed should be $d = 0.221$ nm. This value is in better agreement with the values after 45 min annealing shown in Fig. 10.

The comparison of thermal structural evolution behaviours of 5/5, 8/8, 20/20 and 40/40 samples, as revealed by TEM *in situ* observation and X-ray diffraction, shows that, with increasing layer thickness, the stability against grain growth and coarsening (and thus against destratification) also increases. For grain growth, this is probably due to the difference of lattice strains with layer periodicity. On increasing the layer thickness, the lattice strain and thus the driving force for grain growth decreases. Concerning the coarsening, it may be explained as follows: the enhancement of the diffusion length necessary for the "layer coarsening process" postpones the coarsening.

3.3. Comparison with indirect methods

The appearance of structural relaxation and destratification in Ag–Ni multilayers during heating has been detected by measurements of electrical resistivity and dimension (length) variations by Rodmacq *et al.* [20]. For 6/6 samples, there are two distinct stages during heating:

(i) Above about 100 °C, a non-recoverable resistivity decrease takes place while the length of the sample shows a marked contraction. These effects could be due to local relaxation at the interfaces.

(ii) Beginning at about 350 °C, a drastic resistivity drop is observed; almost concurrent with it, a non-reversible creep starts. This late stage corresponds to destratification.

Recalling our TEM *in situ* heating observation of the 5/5 sample, the lattice strain relaxation begins at about 100 °C and is finished at about 350 °C; in the

350–400 °C temperature range a drastic coarsening of grains takes place and the satellite peaks in X-ray diffraction also disappear to give pure Ag and Ni Bragg peaks: the layered periodicity is destroyed. The TEM and X-ray results are fully consistent with the resistivity and dimension measurements.

4. Summary

1. Ag–Ni multilayers exhibit a dominant [1 1 1] texture in the growth direction. The texture axis may spread over a large angular range ($\sim 20°$). On increasing the layer thickness the angular spread of the texture decreases.

2. When the number of bilayers in the film is small, the in-plane orientations of the grains are at random. An increase of the bilayer number induces sixfold in-plane texture. Ag and Ni grains in a column perpendicular to the layer keep the same orientation.

3. Annealing induces lattice strain relaxation, grain growth and coarsening. The latter finally destroy the periodicity.

4. If the layer thickness is increased, the interfacial coherency and thus the lattice strain decrease, and stabilize the periodic layered structure of the film. In addition, the enhancement of the diffusion length postpones destratification and contributes significantly to multilayer stability.

Acknowledgements

The authors would like to thank Dr B. Rodmacq of CENG for his collaboration. Discussions with Drs J. Hillairet and J. Thibault in CENG have also been very helpful. One of the authors (Y. S. W.) thanks CNRS of France for providing financial support to carry out this project.

References

1. L. L. CHANG and B. C. GIESSEN, "Synthetic Modulated Structures" (Academic, London, 1985).
2. P. DHEZ and C. WEISBUCH, in "Physics, Fabrication and Applications of Multilayered Structures" (North-Holland, Amsterdam, 1988).
3. A. CHAMBEROD and J. HILLAIRET, in "Metallic Multilayers", Materials Science Forum Vol. 59–60 (Trans Tech Publications, 1990).
4. J. L. MAKOUS and C. M. FALCO, *Solid State Commun.* **68** (1988) 375.
5. *Idem, ibid.* **72** (1989) 667.
6. F. J. A. den BROEDER, D. KUIPER, A. P. von de MOSSELAER and W. HOVING, *Phys. Rev. Lett.* **60** (1988) 2769.
7. T. B. MASSALSKI, J. L. MURRAY, L. H. BENNETT and H. BAKER, in "Binary Alloy Phase Diagrams" (American Society for Metals, Metals Park, Ohio, 1986).
8. P. VILLARS and L. D. CALVERT, in "Pearson's Handbook of Crystallographic Data for Intermetallic Phases" (American Society for Metals, Metals Park, Ohio, 1985).
9. B. RODMACQ, *J. Appl. Phys.* **70** (1991) 4194.
10. H. YANG, Y. TAKENAKA, A. ISHIDA and H. FUJIYASU, *ibid.* **68** (1990) 1606.
11. J. C. HEYRAUD and J. J. MÉTOIS, *Surf. Sci.* **100** (1980) 519.
12. B. RODMACQ and J. THIBAULT, in Proceedings of Mater. Research Society Spring Meeting, Anaheim, 1991, Vol. 221, to be published.
13. D. CHERNS, *Phil. Mag.* **30** (1974) 549.
14. B. RODMACQ and J. THIBAULT, Private Communication, 1992.
15. H. DOHNOMAE, N. TAKAYAMA and T. SHINJO, *Mater. Trans. JIM* **31** (1990) 615.
16. J. W. MATTHEWS and A. E. BLAKESLEE, *J. Cryst. Growth* **27** (1974) 118.
17. R. PEOPLE and J. C. BEAN, *Appl. Phys. Lett.* **47** (1985) 322.
18. J. S. LANGER, *Ann. Physik* **65** (1971) 53.
19. L. D. GRAHAM and R. W. KRAFT, *Trans. Met. Soc. AIME* **236** (1966) 94.
20. B. RODMACQ, V. PELOSIN and J. HILLAIRET, in Proceedings of Materials Research Society Spring Meeting, Anaheim, 1991, Vol. 229, p. 97.

Received 6 November 1991
and accepted 2 June 1992